Nucl. Fusion **52** (2012) 033008 (11pp) doi:10.1088/0029-5515/52/3/033008

Measurements of core lithium concentration in a Li-conditioned tokamak with carbon walls

M. Podestà, R.E. Bell, A. Diallo, B.P. LeBlanc, F. Scotti and the NSTX Team

Princeton Plasma Physics Laboratory, Princeton NJ 08543, USA

E-mail: mpodesta@pppl.gov

Received 3 November 2011, accepted for publication 16 February 2012
Published 8 March 2012
Online at stacks.iop.org/NF/52/033008

Abstract

The National Spherical Torus Experiment (NSTX Ono *et al* 2000 *Nucl. Fusion* **40** 557) is exploring the use of lithium as candidate plasma-facing material to handle the large power flux to the wall of fusion devices. This paper reports on the measurements of lithium concentration in the plasma core during the 2010 NSTX experimental campaign, during which 1.3 kg of lithium was evaporated into the NSTX vessel. It is shown that lithium does not accumulate in significant amounts inside the plasma, resulting in an upper bound for the measured lithium concentration that is well below 0.1% of the electron density for a broad range of experimental conditions. Carbon, which constitutes the primary material of the NSTX inner wall, remains the dominant plasma impurity even after large amounts of lithium, of the order of hundreds of milligrams, are evaporated into the vacuum vessel.

(Some figures may appear in colour only in the online journal)

1. Introduction

One of the major challenges for future fusion devices is the handling of large energy fluxes impinging on the vacuum vessel wall [1]. Large fluxes can cause erosion and damage of the plasma-facing components (PFCs). For instance, the steady-state perpendicular heat flux to the divertor surface must be limited to 10 MW m^{-2} for the present ITER design [1]. The choice of the *ideal* material for the PFCs is constrained by two main requirements. From an engineering point of view, the primary goal is to minimize the harm caused to the PFCs by high, possibly intermittent, heat loads. On the physics side, the influx of impurities from the plasma boundary into the core plasma must be kept within acceptable levels to minimize the dilution of the fusion fuel and to prevent an excessive amount of power from being radiated away from the confinement region. Lithium has been proposed as a candidate material to be used as an interface between a carbon or metallic wall and the plasma periphery (scrape-off layer, SOL). Different techniques for applying lithium, ranging from solid lithium evaporated on the PFCs in between shots to liquid lithium somehow contained on *ad hoc* designed limiters or divertor, have been proposed and tested on a number of devices [2–5].

The National Spherical Torus Experiment, NSTX [6], is exploring the possible benefits of lithium as plasma-facing material [7–10]. Experiments aimed at studying the effects of lithium-coated PFCs on the plasma performance were conducted in the past years. The core lithium concentration was measured in 2008 through active charge-exchange recombination spectroscopy (CHERS) for a single operating condition, see figure 8 in [7]. It was concluded that only a very small amount of lithium, of the order of ~0.1% or less of the electron density, accumulated in the core plasma [7]. Since then, a new divertor configuration has been designed and implemented to explore the advantages of a *liquid lithium divertor* (LLD) on the NSTX performance [11], thus motivating further measurements and more detailed analysis of core lithium concentration under a wide range of operating parameters. This paper reports on charge-exchange spectroscopic measurements of lithium concentration in the core plasma during the 2010 experimental campaign. Although no dedicated experiments were performed, data collected throughout the campaign are used to investigate the behaviour of lithium under a variety of conditions. It is shown that lithium does not accumulate in significant amounts inside the plasma. Carbon, which constitutes the primary material of the NSTX inner wall, remains the dominant impurity even after hundreds of milligrams of lithium are evaporated onto the vacuum vessel PFCs.

It is noteworthy to point out that all lithium charge-exchange lines are blended with a corresponding carbon line at nearly the same wavelength. The blending of these two lines

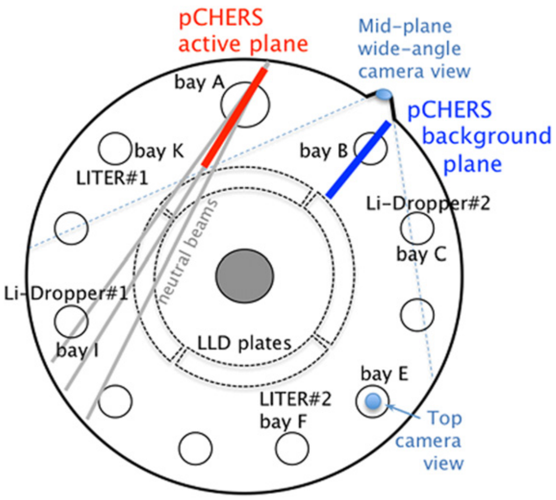

Figure 1. Top view of NSTX showing the position of the main systems used for this work, namely the pCHERS systems for lithium and carbon concentration measurements, the path of the three NB lines, the LITER evaporators, the Li-dropper systems and the LLD plates on the bottom of the machine. Two wide-angle cameras are used to monitor either visible or filtered (Li I, Li II) emission from the plasma edge and SOL.

in NSTX, due to the low lithium content and the relatively large carbon content, makes the exact quantification of the lithium density challenging. A semi-quantitative estimate of the fraction of the emission due to carbon at the lithium wavelength will be presented in section 2.2. Thereafter, the values of lithium concentration reported will refer to the entire emission from the blended lines and so should be interpreted as an upper limit. (Incidentally, similar considerations also apply to previous lithium measurements from NSTX, e.g. those discussed in [7]).

The rest of the paper is organized as follows. Section 2 introduces the experimental setup, including the techniques developed to introduce lithium in the NSTX vessel and the diagnostics used for estimates of the core lithium concentration. Experimental results for high-confinement (H-mode) discharges are described in section 3. A few examples of *anomalous events* leading to abnormally high (for NSTX) lithium content in the plasma are also discussed. Section 4 concludes the paper.

2. Experimental setup

NSTX (figure 1) is a spherical tokamak with major and minor radius $R_0 = 0.85$ m and $a \leqslant 0.65$ m. The aspect ratio is 1.3–1.5. It operates with a toroidal field in the range 3.5–5.5 kG, plasma current of the order of 1 MA and deuterium as the main ion species. Typical densities are $(3\text{–}10) \times 10^{19}\,\mathrm{m}^{-3}$, with central electron and ion temperature $T_e \approx T_i \sim 1$ keV. Neutral beam (NB) injection is the primary system for plasma heating and current drive. The maximum available power is $P_{NB} = 7$ MW. The range of injection energies is 60–90 keV. The injected neutral species is deuterium.

NSTX plasmas are mostly run in a lower-single-null, diverted configuration with the strike point on the bottom divertor region. The NSTX inner wall is primarily covered by graphite tiles, which makes carbon the main PFC. A novelty during the 2010 experimental campaign was the introduction of a LLD system installed on the outer region of the lower divertor [11] (see the next section).

2.1. Li conditioning techniques on NSTX: LITER, Li-dropper and LLD

Over the past years, different techniques have been deployed to introduce lithium into the NSTX vessel. For most of the discharges, lithium is evaporated into the vessel prior to a plasma discharge from two *lithium evaporators* (LITERs, see [12, 13] and references therein), located on the top of the vessel and ≈180° apart toroidally, see figure 1. The evaporation rate is adjustable, with a maximum of 70 mg min^{-1} and typical rates of 5–15 mg min^{-1} for 5–10 min in between discharges. In practice, LITER operation can maintain good wall conditions and increase the repetition rate from 4 shots per hour to 6 shots per hour by eliminating the need for in-between-shot PFC conditioning using helium glow discharge. A further increase in shot rate is limited by other engineering constraints, for instance the cooling time of the magnetic field coils. Lithium evaporation during the machine start-up after prolonged vents has also eliminated the need for boronization and reduced the re-commissioning time [7].

A second and more localized technique to introduce lithium makes use of a *lithium dropper* (Li-dropper) [14] to release small lithium granules from the top of the machine. The granules are made of metallic lithium encapsulated by a thin mantle of Li_2CO_3. The average diameter is 44 μm, which corresponds to a mass of ≈23 μg. Two systems, installed at two opposed toroidal locations, were operational on NSTX in 2010 (figure 1). Each system is aimed at different plasma regions, namely the outer edge or the inner edge close to the centre column. The Li-dropper systems allow controlled quantities of lithium to be introduced either before or during a discharge, even for short periods (tens of milliseconds), in contrast to the continuous evaporation from the LITER systems.

The LITER and Li-dropper (used before a discharge) deposit lithium mainly on the PFCs in the bottom region of the NSTX vacuum chamber, which is where most of the plasma–wall interactions occur. Four LLD divertor plates have been installed inside the vessel prior to the 2010 NSTX experimental campaign on the lower-outer divertor to test the advantages of liquid over solid lithium on the PFCs [11]. The LLD plates cover a full 360° toroidal angle and span ≈20 cm radially, between $R = 65$ cm and $R = 85$ cm in major radius [15]. The plates are covered by a layer of porous molybdenum that traps up to 37 g of lithium. The plates can be heated above 180 °C (i.e. the nominal melting temperature of pure lithium), so that the plasma at the divertor is in contact with a liquid lithium film. In general, the advantage of liquid over solid lithium resides in the possibility of a continuous refurbishment of the lithium-coated surface, for instance through capillary systems. A LLD would in principle maintain its properties for long periods of time (≫1 s), as required for (ideally) steady-state operations of a fusion reactor [16, 17]. LLD refurbishment through capillarity is under consideration [10] for long-pulse (up to ∼5 s) scenarios of the NSTX Upgrade [18].

Table 1. Summary of NSTX charge-exchange spectroscopic diagnostics used for carbon and lithium concentration measurements.

System	CHERS	pCHERS	Li-pCHERS
Views	Tangential	Vertical	Vertical
Measured/ derived quantities	n_C, $v_{\rm tor}$ n_i, $T_{\rm i}$, $Z_{\rm eff}$	n_C, $v_{\rm pol}$	$n_{\rm Li}$ $n_{\rm Li}/n_C$
Monitored species	C VI	C VI	Li III C VI C II
Monitored lines	5290.5 Å	5290.5 Å	5166.89 Å (Li III) 5166.67 Å (C VI) 5151.1 Å (C II)
Radial coverage	90–157 cm	90–157 cm	120–157 cm

2.2. Core lithium concentration measurements: diagnostic techniques

Table 1 provides a summary of the suite of CHERS diagnostics installed on NSTX and used in this work. Each system consists of a fixed-wavelength spectrometer coupled to a charge-coupled device (CCD) detector with sampling rate of 100 Hz. During the 2010 NSTX run, two of the six vertically viewing (or *poloidal*) CHERS systems commonly used to measure carbon [19] were converted to measure the lithium concentration in the core plasma by substituting transmission gratings to measure Li III emission. Light is collected from NSTX plasmas through optical fibres and transported from the NSTX test-cell to a separated diagnostic room, thus minimizing noise from gamma and neutron radiation. Two sets of views are used to separate the *active* (charge-exchange) lithium emission from the region intercepting the heating NB from the *passive* (or background) contribution, see figure 2. The latter set of views is toroidally displaced with respect to the volume illuminated by the NB (figure 1).

The *lithium-poloidal-CHERS* (Li-pCHERS) spectrometers measure in the radial range $R \approx 120$–155 cm with a temporal resolution of 10 ms, in the wavelength range 5145–5180 Å (figure 3). A second set of pCHERS views, looking at C VI emission ($n = 8 \rightarrow 7$ transition at 5290.5 Å), is interleaved with the Li-pCHERS views. Views looking at the same portion of the plasma, radially and toroidally, share the same optics.

The emission line used to infer lithium concentration is the Li III line at rest wavelength in air of 5166.89 Å ($n = 7 \rightarrow 5$ transition)[1]. Other prominent emission lines in the same spectral range are a C II line at 5151.08 Å, a C VI line at 5166.67 Å and a molecular band of C_2, called the Swan band [20], extending from ≈5150 Å up to 5165.25 Å (figure 3). The Swan band, and in particular its head-band lines, partly overlaps the Li III line. Therefore, a simultaneous least-squares fit of both lines is required to infer the lithium emission from the measured spectra.

The major source of uncertainty in the accurate determination of the lithium brightness is caused by the C VI line ($n = 14 \rightarrow 10$ transition, $\lambda = 5166.67$ Å) located at the same wavelength as the Li III line of interest. The result is a possible blend of up to four lines contributing to the measured spectra at comparable wavelengths, namely the active (charge-exchange) Li III and C VI lines and their background counterparts. The exact shape of the measured spectrum depends on the line-integral along a specific line of sight of contributions with possibly different brightness, temperature and velocity. Such a multiplet, that appears further broadened on the CCD detector because of the instrumental function of the spectrometer, cannot be unambiguously resolved through a multi-line fit of the spectrum without additional constraints to the fit.

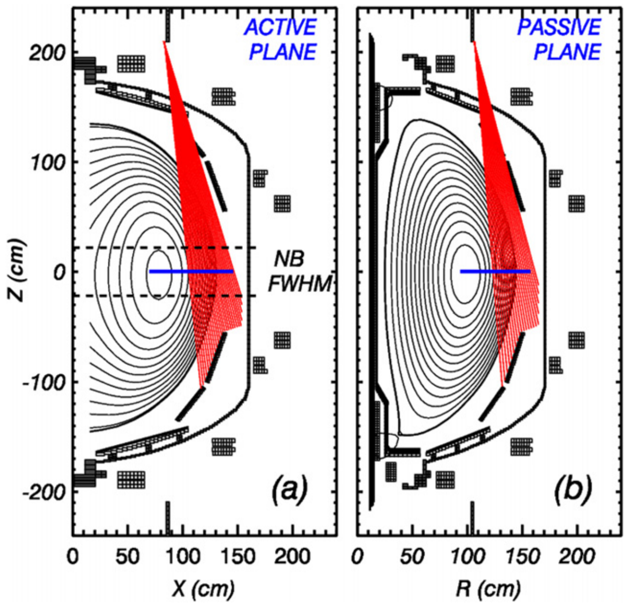

Figure 2. Overview of the pCHERS views used for measurements of lithium. Shown are (*a*) the *active* plane along the path of the NB source B and (*b*) the *passive*, radial plane at bay B used for background measurements. The thick blue line at mid-plane ($Z = 0$) in each panel indicates the range covered by the main (toroidal) CHERS views.

Since a considerable amount of lithium was already introduced in NSTX during the machine re-commissioning in 2010, no *lithium-free* comparison discharges are available for NSTX. Ideally, one would like to use the measured C VI, $n = 8 \rightarrow 7$ transition to estimate the brightness of the C VI, $n = 14 \rightarrow 10$ transition. This would require either a direct measurement in a lithium-free plasma, or an accurate collisional radiative model to predict the relative populations of the $n = 14$ and $n = 8$ levels in carbon. For example, the two carbon lines were measured simultaneously during the commissioning of the TFTR poloidal rotation diagnostic [21]. The measured carbon spectra indicate that the fraction of C VI for the $14 \rightarrow 10$ transition with respect to the $8 \rightarrow 7$ transition is ≈3.6% for electron density and temperature of $\sim 1.2 \times 10^{19}$ m^{-3} and ~3 keV. In order to relate TFTR results to the spectra measured on NSTX, a collisional–radiative model for C VI is used to check whether the ratio between populations of different n levels is sensitive to variations in density and temperature. The model, described in [21], is used to calculate the relative population of the $n = 1$–20 levels for C VI. The source term is set by the population of the n levels from charge-exchange with $n_{\rm D} = 1$–3 donor neutrals. A set of

[1] Wavelengths of spectral lines from Atomic Line List, http://www.pa.uky.edu/~peter/atomic

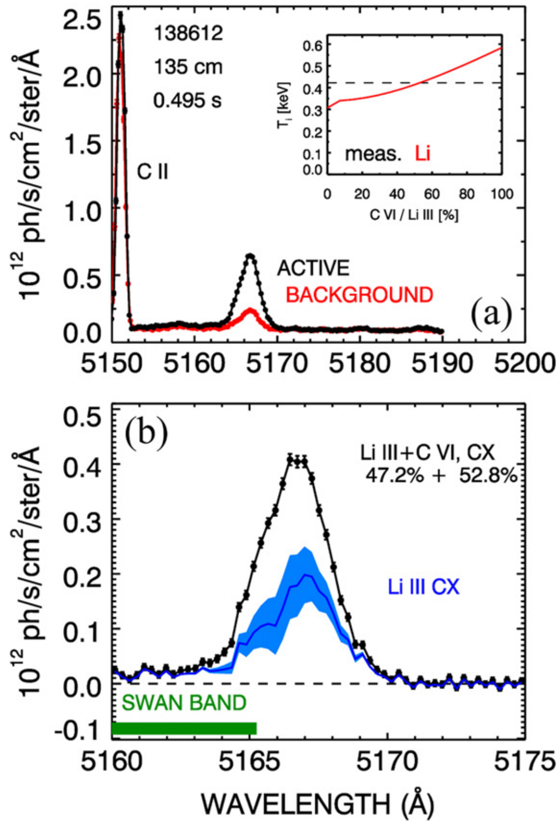

Figure 3. Example of spectrum measured by the Li-pCHERS system. (*a*) Spectrum measured by a sightline intercepting the NB (*active*) and missing the NB (*background*). The inset shows the inferred line-integrated temperature for Li III at 5167 Å as a function of the relative amplitude between the brightness of the active charge-exchange C VI and Li III lines. Results are consistent with the temperature measured for the C VI, $n = 8 \rightarrow 7$ line assuming that C VI, $n = 14 \rightarrow 10$ constitutes ≈50% of the brightness measured at 5167 Å. (*b*) Details of the active spectrum after subtraction of the background and of the charge-exchange (CX) contribution from C VI. The band for the net Li III spectrum indicates the estimated uncertainties of ±25%.

differential equations, coupled through transition probabilities from ionization, excitation/de-excitation and radiative cascade from other levels, is evolved in time until a steady-state is reached. Using the transition probabilities for the measured transitions, the relative brightness of the $n = 14 \rightarrow 10$ to the $n = 8 \rightarrow 7$ carbon lines can be determined, along with its dependence upon density and temperature. The modelled relative brightness ratio for the TFTR case is ≈0.9%, that is about 4 times smaller than the measured value. The model is inadequate to reproduce the measured value, presumably due to inadequate population terms of the upper levels of carbon from charge exchange. Although absolute values are not correctly reproduced, the weak dependence of the results on plasma density and temperature over the range of NSTX plasma parameters suggests that the ratio for NSTX plasmas should be comparable to the ≈3.6% value measured on TFTR, indicating that the expected brightness from C VI for NSTX is an appreciable fraction of the total measured brightness at Li III wavelength.

A more quantitative estimate of the relative contribution from Li III and C VI emissions to the measured active brightness can be independently obtained by fitting the line around 5167 Å under the assumptions that both Li III and C VI contribute to the active charge-exchange signal and that both ion species are at the same temperature, T_i. (The active components represent the temperature of the fully stripped Li IV and C VII ions.) Since the full-width at half-maximum (FWHM) of the peak for a single species depends on both temperature and mass, FWHM $\propto (T_i/M)^{1/2}$, different ion species at the same temperature will result in a different broadening of the observed line. Because the fit is performed on line-integrated spectra, an effective temperature T_i^{eff} is first calculated from the pCHERS views measuring C VI ($n = 8 \rightarrow 7$) that are interleaved with the Li-pCHERS views. The same fit also provides the C VI wavelength, possibly shifted from its rest value by rotation, which is used to calculate the actual C VI ($n = 14 \rightarrow 10$) wavelength based on the difference between nominal C VI rest wavelengths. After background subtraction, the spectrum around 5167 Å, including the Swan band, is then analysed. A fixed wavelength for the C VI ($n = 14 \rightarrow 10$) line and a common temperature for lithium and carbon are imposed, thus reducing the number of free parameters in the fit. The C VI to Li III brightness ratio is varied, until the temperature from the fit is consistent with T_i^{eff}. This provides an estimate of the relative contribution to the brightness from carbon and lithium, see figure 3, indicating that ≈50% of the measured brightness is due to carbon. Uncertainties in the relative C VI to Li III brightness are estimated to be ±25%. The fraction of C VI for the $14 \rightarrow 10$ transition with respect to the $8 \rightarrow 7$ transition can also be calculated. It varies with radius and time in the range 2–6%, in qualitative agreement with the measurement from TFTR. This analysis demonstrates that there is a significant blending due to C VI, although the exact fraction due to carbon is difficult to quantify. For practical purposes, the entire emission of the active signal will be treated as being only from lithium in the following discussion. The resulting values of lithium density must then be interpreted as upper limits rather than quantitatively exact values.

Once the relative brightness from Li III is determined, the C VI emission measured by the carbon pCHERS views is used to re-scale the active spectra based on the absolutely calibrated C VI emission from the main (toroidal) CHERS. This step allows the normalization of the original line-integrated data to *local* density measurements. The integration path is determined by the intersection of each sightline with the NB footprint (figure 2), whose vertical extent is ≈42 cm. Because each sightline collects light from multiple flux surfaces, the actual profile is smeared over ∼3–5 cm along the radial direction (cf figure 3 in [19]) outside $R = 120$ cm. The latter value, which roughly corresponds to the mid-radius for NSTX plasmas, represents the innermost radius for the lithium measurements discussed in this work.

As a final step in the analysis, a correction of the raw data for the local charge-exchange rate of lithium is performed. An average scaling factor is derived as a function of radius from a sub-set of discharges by comparing the results of a full analysis, including inversion of the profiles, with the non-inverted profiles. The inversion technique to obtain the local emission is similar to the technique described in [19]. It includes an inversion of both the active and background brightnesses to obtain the local values. After background subtraction, the

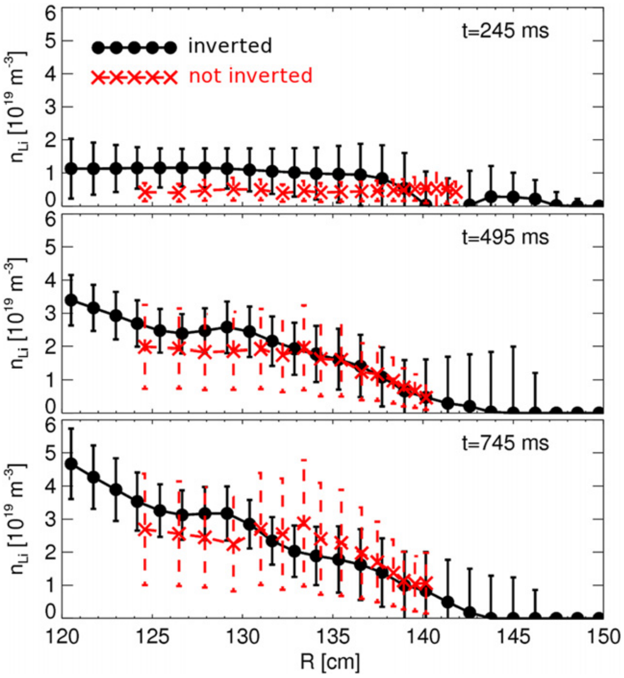

Figure 4. Comparison between non-inverted (red, dashed) and inverted (black, solid) lithium density profiles for three times during discharge no 138612 (cf figure 5). For the purpose of this work the agreement is sufficiently good, although details on the shape of the profiles is partly lost when line-integrated data are used.

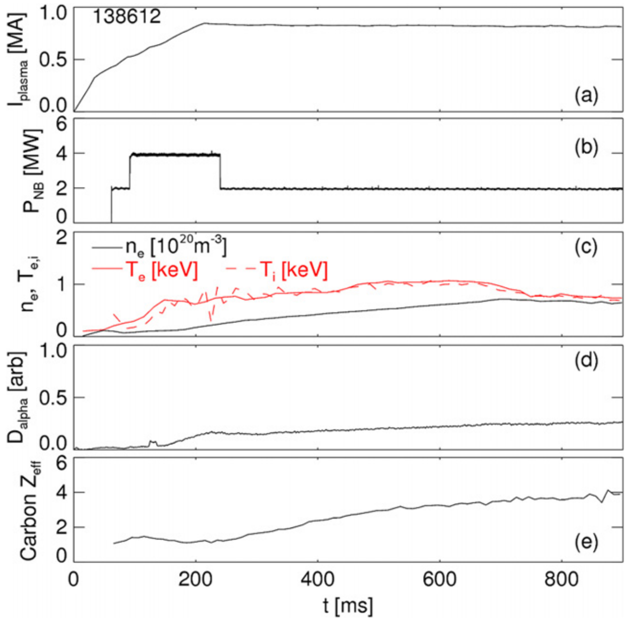

Figure 5. Overview of parameters for shot no 138612: (*a*) plasma current, (*b*) injected NB power, (*c*) central electron density and ion/electron temperature, (*d*) D-alpha emission from the divertor. (*e*) Central Z_{eff}, calculated from CHERS data under the assumption that carbon is the dominant impurity.

local concentration is calculated taking into account the NB deposition profile and the charge-exchange cross sections for each impurity species (i.e. carbon and lithium).

The error bars shown in the figures are the result of uncertainties propagated through the analysis described here above. They include statistical photon noise, uncertainties in the interpolation of spectra from different detectors and shot-to-shot variability in the calculated (average) charge-exchange rates. A comparison of line integrated versus inverted profile is shown in figure 4. The line-integrated measurements are representative of the general features of lithium evolution, such as average concentration and trends with plasma parameters. In the following, only results from the re-scaled, line-integrated data are shown.

3. Upper bounds for Li concentration in H-mode, NB-heated plasmas

NSTX can operate with a large variety of plasma configurations and operational parameters such as toroidal field, plasma current, injected NB power and amount of lithium deposited on the PFCs. A set of discharges from the 2010 experimental campaign has been selected to represent the NSTX operating space for high performance, H-mode plasmas. Preference is given to sequences where a minimum number of parameters are varied in a systematic way. Representative discharges of all lithium application techniques (i.e. LITER, Li-dropper, LLD) are examined. In view of an upgrade of the NSTX device to higher toroidal fields and plasma currents (NSTX-U, see [18]), leading to slightly larger aspect ratio, scans of those parameters are also included in the selected database. Discharges with injected NB power $2 \leqslant P_{\mathrm{NB}} \leqslant 4$ MW have been preferentially selected. Limiting the injected power to $\lesssim$4 MW helps us to avoid disruptions caused by reaching an upper limit in the plasma β (ratio of plasma kinetic energy to magnetic energy). Discharges with large MHD activity are discarded from the data set. The presence of large MHD modes may obscure trends derived from a shot-to-shot scan of a specific parameter, since such modes may appear in a non-reproducible fashion in the different discharges. The main results from the analysis of core lithium concentration are presented in the next sections.

3.1. *Evolution of lithium concentration for standard NSTX discharges*

A typical NSTX discharge with low-power NB injection and deuterium fuelling is shown in figure 5. The target discharge has plasma current $I_{\mathrm{plasma}} = 0.8$ MA and toroidal field on axis $B_{\mathrm{tor}} = 4.5$ kG. The injected NB power is $P_{\mathrm{NB}} = 2$ MW, except for a short pulse with $P_{\mathrm{NB}} = 4$ MW during the current ramp-up to favour access to H-mode. The transition to H-mode occurs at $\sim$150 ms, during the current ramp-up. A phase with relatively stationary plasma parameters starts soon after, although a rise in electron density is observed throughout the entire discharge. Central electron and ion temperatures are around 1 keV. The plasma remains in a lower-single-null, diverted configuration for the entire discharge. Low MHD activity is measured during the current ramp-up, followed by a quiescent period between 300 ms and $\approx$700 ms. One of the salient features observed in discharges with lithium evaporation is apparent from figure 5(*d*), showing a D-alpha trace from the plasma edge. The absence of spikes in the time trace reveals that edge-localized modes (ELMs) are not de-stabilized, as observed with large lithium evaporation rates [9, 22]. As a drawback, the impurity content in the plasma core undergoes a secular

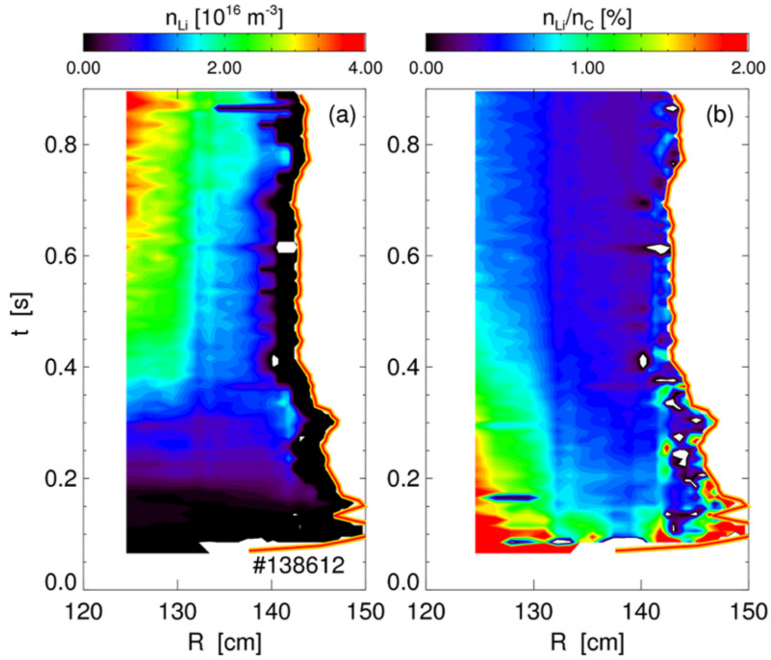

Figure 6. (*a*) Upper limit of lithium density, inferred from line-integrated data, and (*b*) ratio of lithium-to-carbon concentrations for shot no 138612 (see figure 5 for the main plasma parameters), corresponding to a standard H-mode NSTX discharge. The red line indicates the radius of the separatrix at mid-plane, as calculated through the equilibrium code EFIT. The analysis is performed using an average correction factor for the different charge-exchange rates between C VI and Li III.

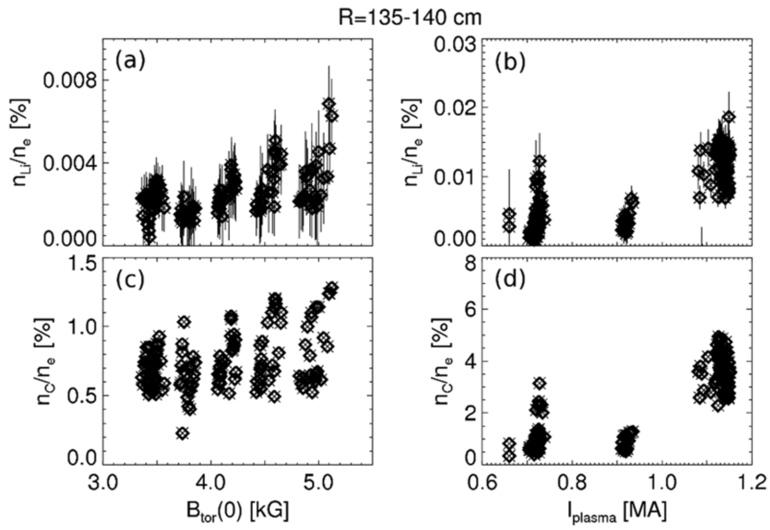

Figure 7. Lithium (*a*)–(*b*) and carbon (*c*)–(*d*) concentration as a function of toroidal magnetic field for a fixed $I_{plasma} = 0.9$ MA (left column) and of plasma current for a fixed $B_{tor} = 5.5$ kG (right column). Measurements shown here are from the time window $t = 250$–400 ms.

increase, with an effective charge of $Z_{eff} \geqslant 3$ after 500 ms (figure 5(*e*)). (Values of Z_{eff} shown here are calculated under the assumption that carbon is the dominant low-Z impurity, which is usually a good assumption for NSTX plasmas).

The temporal evolution of the lithium density profile for the discharge in figure 5 is shown in figure 6(*a*). It can be seen that the profile starts to build up after the transition to H-mode at $\approx$150 ms. Nevertheless, the absolute lithium density is low compared with both the main ion (deuterium) and carbon density. The ratio between lithium and carbon concentration is reported in figure 6(*b*), showing that lithium concentration remains below 2% of the carbon density and $\ll$0.1% of the electron density during the entire discharge.

3.2. *Scan of toroidal field, plasma current and aspect ratio*

The generality of the results shown in figure 6 is investigated by varying the discharge conditions, namely the toroidal magnetic field and the plasma current. The results are shown in figure 7. A weak trend is observed with both toroidal field and plasma current, resulting in an increase in the average impurity content with increasing B_{tor} and I_{plasma}. The increase in impurity level is consistent with a general improvement of confinement for

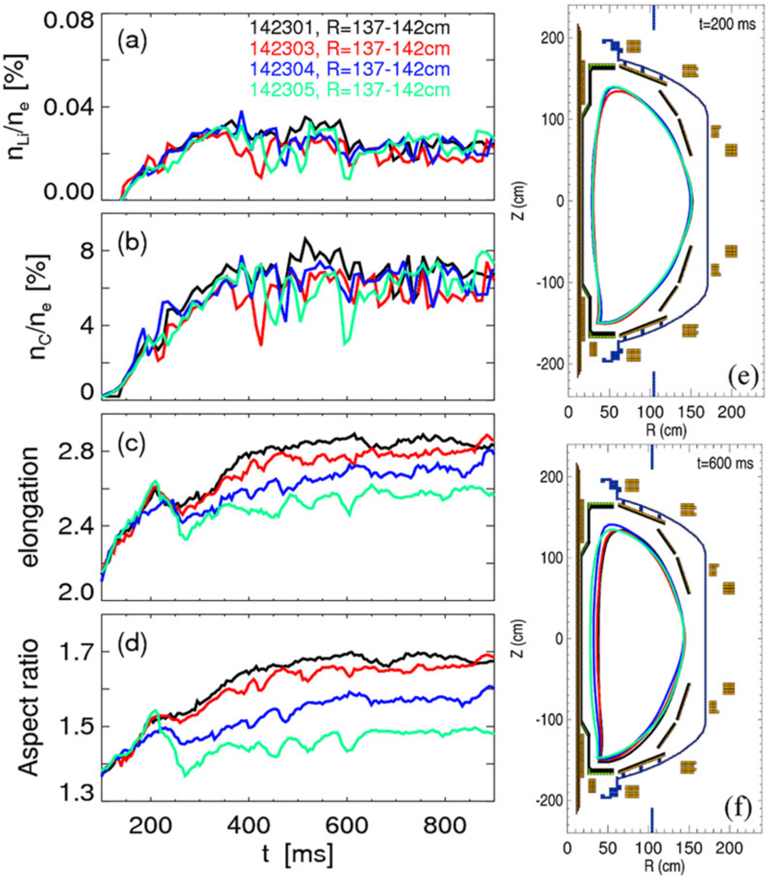

Figure 8. Ratio of (*a*) lithium and (*b*) carbon concentrations over electron density as a function of the aspect ratio. The time evolution of plasma elongation and aspect ratio is shown in (*c*) and (*d*). The plasma configuration is the same for all four discharges up to the end of the current ramp-up at $t = 200$ ms, then is varied during the current flat-top. (*e*)–(*f*) Cross-section of NSTX with plasma separatrix at two different times corresponding to the end of the current ramp-up ($t = 200$ ms) and the flat-top, stationary phase ($t = 600$ ms). Note that the decrease in lithium concentration after 600 ms shows a distinctively different history than carbon, indicating a substantial fraction of the brightness at the nominal Li III wavelength is indeed lithium.

higher magnetic field and current [23]. For future devices with higher field than NSTX, including the planned NSTX-U, the implications of this unfavourable scaling for accumulation of impurities in the core plasma are an issue that needs to be addressed, cf [24–26].

Another parameter of interest in view of projections of the NSTX results to future devices is the aspect ratio. For instance, several studies in 2010 have focused on the dependence of plasma parameters, stability and performance on the aspect ratio in view of an upgrade of the NSTX device [18]. The planned NSTX-U implies a larger centre column, leading to larger aspect ratio for standard configurations. Larger aspect ratios are obtained on NSTX by increasing the gap between the centre column and the plasma boundary at the high-field side. A comparison of impurity content to the aspect ratio and plasma elongation is shown in figure 8 for four discharges with aspect ratio increasing from ∼1.4 (average value for present NSTX plasmas) up to ∼1.65 (projected value for NSTX-U), see figure 8(*d*). The plasma elongation (figure 8(*c*)) also changes with the aspect ratio.

No substantial variation of the lithium core concentration is measured when the aspect ratio, hence the gap between plasma and centre column, is varied (figures 8(*a*) and (*b*)). These results may suggest that the gap size does not strongly influence the influx of impurities due to enhanced sputtering from the centre stack tiles. Another important observation is that the four discharges follow the same trajectory during the start-up and ramp-up phases, up to $t \approx 200$ ms (figure 8(*e*)), then the magnetic configuration is varied to achieve the desired value of aspect ratio during the current flat-top (figure 8(*f*)). This may suggest that impurity accumulation during the discharge does depend, among other factors, on the initial evolution of the discharge. For instance, the initial breakdown on NSTX happens close to the centre column, then the plasma grows in a limited (on the inner wall) configuration. Therefore, sputtering and erosion of the PFCs may occur during this initial phase at a higher rate than during the flat-top, when the plasma is diverted and interactions with the PFCs should be reduced.

3.3. *Li concentration for different Li conditioning techniques*

Although the LITER systems are mostly used for NSTX operations, it is worth studying the effect on NSTX plasmas of the other lithium-conditioning techniques introduced in section 2.1. In principle, the different techniques may be associated with different impurity source terms, which in turn may influence the amount of lithium (and carbon) that accumulates in the inner plasma regions. For this purpose, it is

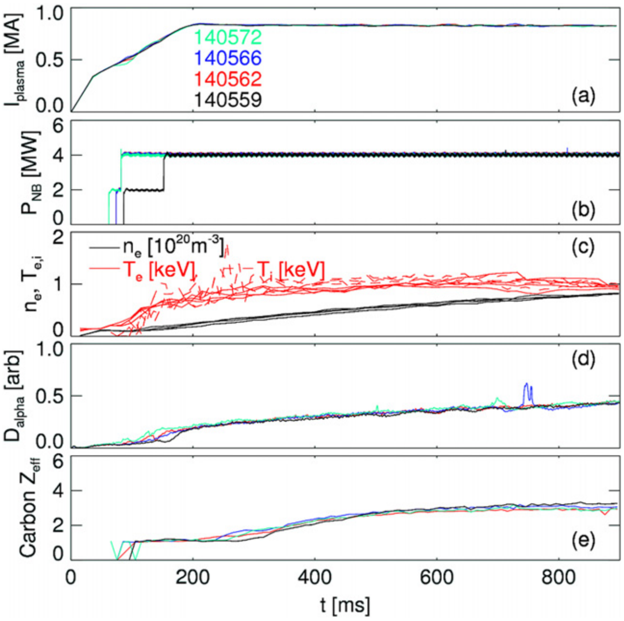

Figure 9. Main parameters for four discharges utilizing different lithium-conditioning techniques: (*a*) plasma current, (*b*) injected NB power, (*c*) electron density and ion/electron temperature, (*d*) D-alpha emission from the divertor and (*e*) central Z_{eff} from carbon. The amount of lithium delivered by either the LITER or the Li-dropper systems is reported in table 2. Plasma parameters are not strongly affected by the different methods used to condition the NSTX PFCs prior to each discharge.

Table 2. Total amounts of lithium deposited from Liter and lithium dropper for the discharges in figure 11. For the Li-dropper, the first value in the sum corresponds to the amount of lithium pre-positioned before the discharge and the second value to the amount released during the discharge.

Shot no	LITER	Li-dropper
140559	240 mg	—
140562	240 mg	240 mg + 240 mg $\mathrm{s^{-1}}$ $\times$ 1.2 s
140566	240 mg	0 mg + 100 mg $\mathrm{s^{-1}}$ $\times$ 1.1 s
140572	120 mg	240 mg + 120 mg $\mathrm{s^{-1}}$ $\times$ 1.2 s

useful to explore the possible differences when the conditions at the plasma–wall boundary are changed. Four discharges are investigated, whose main parameters are summarized in figure 9. The four discharges exhibit very similar plasma parameters, although different amounts of lithium are inserted from either the LITER or the Li-dropper systems before and during the discharge. In addition to toroidal field, plasma current and plasma parameters, other quantities discussed later, such as the vertical plasma position and the height of the lower *X-point* above the divertor (*bottom gap*), are reasonably close for the different shots, cf figures 11(*c*) and (*d*). The plasma magnetic configuration is also very similar for these four discharges. A fish-eye camera view of the NSTX plasma during a discharge with lithium injection from the Li-dropper throughout the discharge is presented in figure 10, which shows that lithium granules can, in fact, interact with the plasma in the SOL and at the plasma edge. In spite of this, a similar lithium concentration is measured in the core for discharges with lithium evaporation from LITER prior to the shot, with lithium from the Li-dropper or with both together (figure 11). Consistently with the lithium results shown above, the carbon

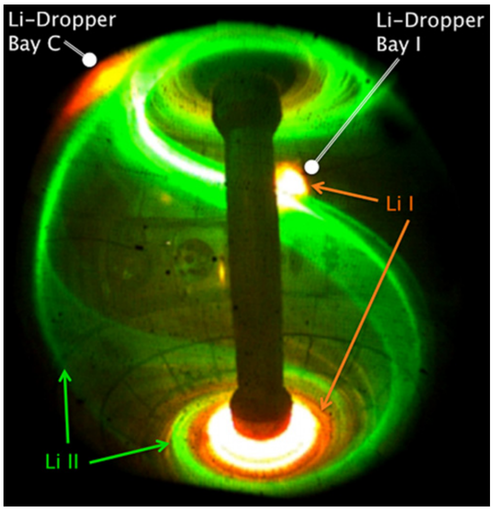

Figure 10. Fish-eye camera view of the NSTX chamber from a mid-plane port (cf figure 1). Data refer to discharge no 140572, with both Li-dropper systems releasing lithium during the shot. The red, more localized spots are caused by Li I emission from the SOL. The green stripes that follow the magnetic field line structure are caused by Li II, which can penetrate a few centimetres inside the separatrix.

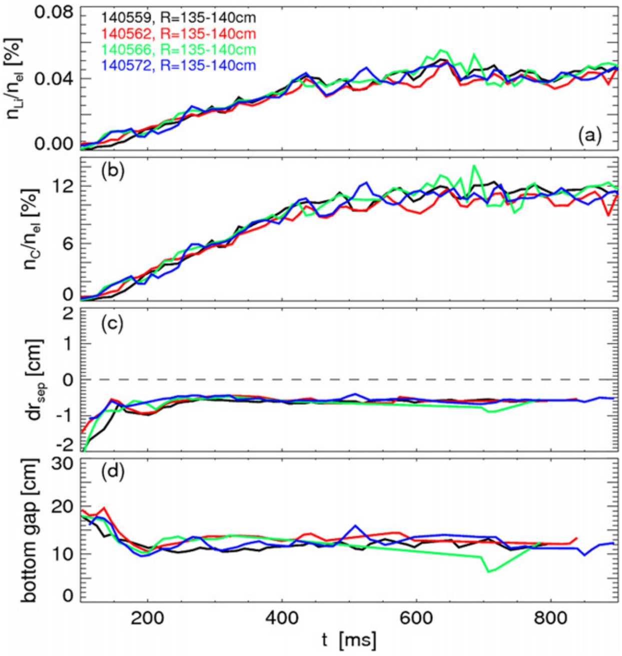

Figure 11. Time evolution of the ratio of (*a*) lithium and (*b*) carbon concentrations over electron density measured at the plasma edge for different lithium-conditioning techniques (Liter, Li-dropper). The specific conditions for the different discharges are summarized in table 2. The evolution of (*c*) dr_{sep} and (*d*) bottom gap for these discharges does not show substantial differences, indicating that the plasma configuration is very similar.

concentration does not vary significantly among the different discharges (figures 9(*e*) and 11(*b*)). On the other hand, it is known from NSTX experiments that lithium conditioning of the PFCs has some cumulative effect if LITER is used for many consecutive discharges at high ($\gtrsim$40 mg $\mathrm{min^{-1}}$ total from two evaporators) evaporation rates. It is therefore possible that, although the Li-dropper systems are releasing an amount of lithium comparable to the one from LITER, the dominant

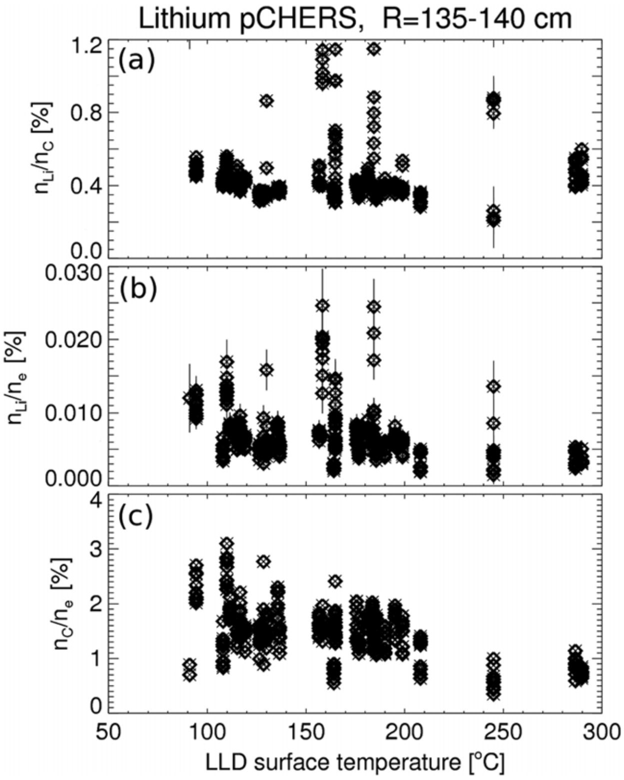

Figure 12. Ratio of (*a*) lithium-to-carbon concentrations and (*b*)–(*c*) their relative concentrations with respect to the electron density measured at the plasma edge as a function of the LLD surface temperature. Data from each discharge are selected during the current flat-top phase between 500 and 600 ms, when the LLD surface temperature is measured.

lithium *reservoir* is still constituted by evaporated lithium from LITER that has accumulated on the PFCs from previous shots.

As a further step, the effect of the divertor conditions on the core lithium concentration is explored. As mentioned in section 2.1, a prototype LLD, covering the lower outboard divertor region, was tested on NSTX during the 2010 Run. By varying the LLD plate temperature, $T_{\rm LLD}$, one can in principle control whether the plasma at the lower divertor is in contact with solid or liquid lithium. As a reference, the nominal melting temperature for metallic lithium is 180 °C. The temperature of the four LLD plates was ramped from low temperature (≈100 °C, which implies solid lithium) up to ≈300 °C (liquid lithium) by positioning the lower strike point on the LLD plates. On average, heating from the plasma is sufficient to increase the temperature at a rate of ∼10 °C shot^{-1}. The measured core lithium density for different values of the LLD plates' temperature is shown in figure 12. The lithium-to-carbon ratio remains roughly constant for different plate temperatures, although both lithium and carbon relative concentrations decrease by a factor ≈2 for $T_{\rm LLD} \gtrsim 200$ °C. Note that the fuelling rate was also much larger for these discharges, so that effects others than a liquid lithium PFC, for instance due to different plasma edge or SOL conditions such as a colder SOL, cannot be ruled out completely to explain this drop. Along with the previous observations of a similar behaviour for different lithium-conditioning techniques, these results indicate that lithium in the core plasma is rather insensitive to the specific characteristics of the PFCs (solid

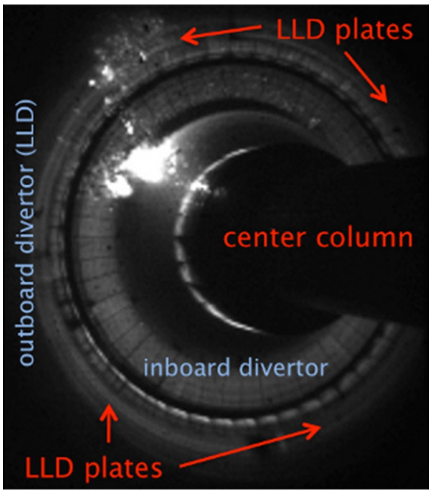

Figure 13. Camera image of Li I emission at 670 nm from discharge no 139681. The camera view looks at the lower divertor from a top port at bay-E (cf figure 1). The bright spots in the upper-left quadrant are the result of the plasma interacting with a macroscopic lithium conglomerate at $t \approx 260$ ms, similarly to what is shown later in figure 16. The discharge disrupts shortly after, at $t \approx 350$ ms.

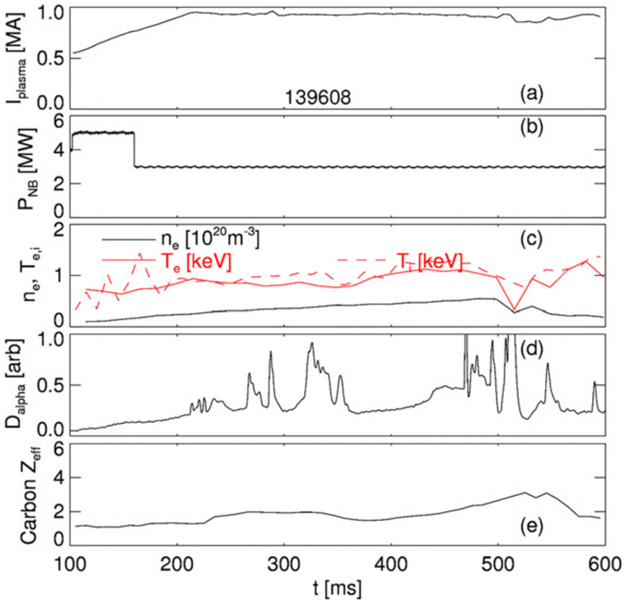

Figure 14. Parameters for NSTX discharge no 139608: (*a*) plasma current, (*b*) injected NB power, (*c*) electron density and ion/electron temperature, (*d*) D-alpha emission from the divertor and (*e*) central $Z_{\rm eff}$ from carbon.

or liquid) and to the details of the plasma–wall interactions in the divertor region.

3.4. Li concentration during anomalous events

A partial conclusion from the previous sections is that the lithium concentration in the core plasma of NSTX remains low, typically around or below 0.1% of the carbon concentration, regardless of the details of the discharge. In this section, we discuss an example of special events that lead to relatively large (for NSTX) lithium concentrations. Such an anomalous event, directly associated with lithium, is the interaction of the plasma with a macroscopic conglomerate of lithium that

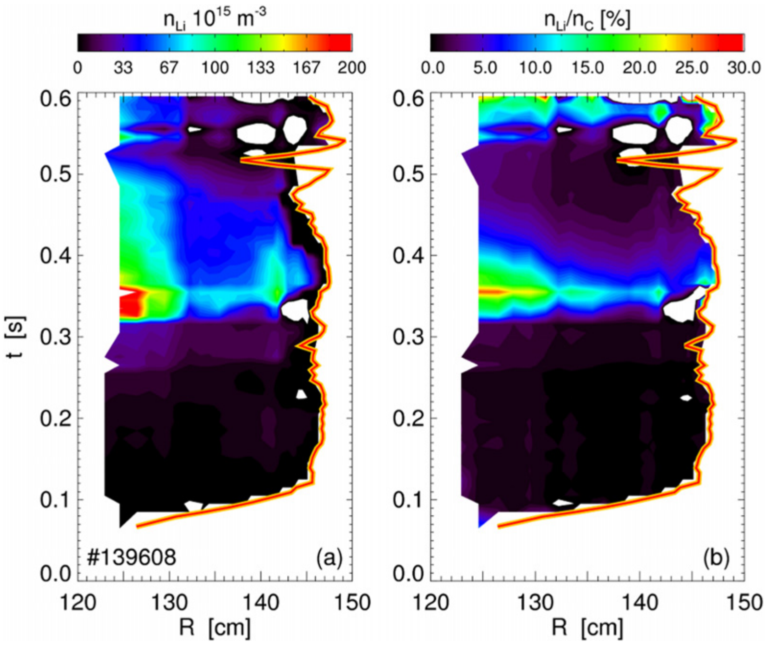

Figure 15. (*a*) Upper limit for lithium density and (*b*) ratio of lithium-to-carbon concentration during plasma interaction with *blob* on lower divertor (NSTX discharge no 139608). Note the difference in the scale used for displaying n_{Li} with respect to typical discharges, e.g. the one shown in figure 6. The red line indicates the position of the plasma separatrix.

accidentally fell on the lower divertor plate from the LITER port during plasma operations. The footprint of the lithium piece, as deduced from camera images of the lower divertor (cf figure 13), has a surface of a few square centimetres. The discharge parameters for one of these shots are shown in figure 14. The NB power is increased up to 5 MW during the current ramp-up, then is lowered to $P_{NB} = 3$ MW when the current reaches its target value of 900 kA (figures 14(*a*) and (*b*)). The secular density increase, with $T_e \approx T_i \approx 1$ keV, is shown in figure 14(*c*). ELMs are virtually absent during most of the flat-top phase (300 ms to ~500 ms, figure 14(*d*)), which results in values $Z_{eff} \sim 3$ from carbon at the end of the pulse.

The corresponding evolution of lithium concentration is shown in figure 15. The evolution is similar to what already discussed in figure 6 up to ≈300 ms, when the outer strike point moves to the divertor region where the lithium conglomerate is located. From this time on, lithium concentration starts to increase at a much faster rate than in normal discharges (note the different colour scale between figure 6 and figure 15). Bursts of lithium are observed at $t \approx 350$ ms and $t \approx 550$ ms, see figure 16, anticipating a disruption that causes the termination of the discharge. The maximum estimated lithium concentration is $n_{Li}/n_e \gtrsim 0.2\%$, with $n_{Li}/n_C \gtrsim 25\%$ and $n_C/n_e \sim 1\%$.

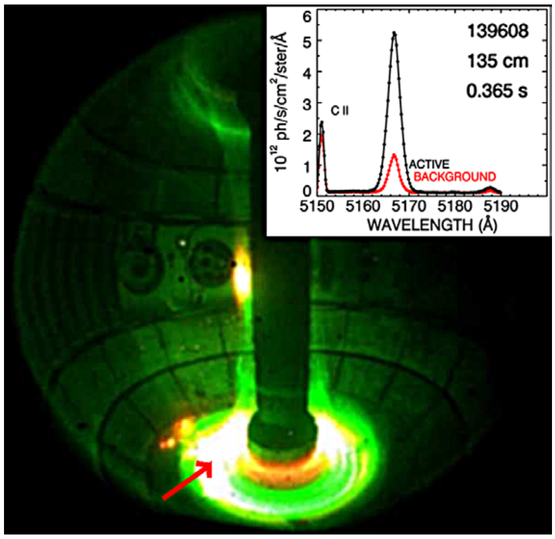

Figure 16. Fish-eye camera image of visible light from discharge no 139608, showing the plasma interacting with a large fragment of lithium on the lower divertor (red arrow) at $t \sim 370$ ms. Red light is neutral Li emission. Green light at the plasma edge is from Li II emission. The bright spot close to the centre column at mid-height is emission from the injected fuelling gas that ionizes in the SOL. The inset shows the dominant Li III peak measured at $R = 135$ cm around $t = 365$ ms. Here the contribution of C VI to the brightness is negligible in comparison with figure 3.

4. Conclusions

A dedicated charge-exchange recombination spectroscopy system has been used to monitor the core lithium concentration throughout the 2010 NSTX experimental campaign. Because of a blending between lithium and carbon lines in the measured spectra, the inferred lithium concentrations are upper limits. The actual values may be lower by a factor of 2 or more.

It is found that extremely low lithium concentrations are a robust property of NSTX plasmas over a wide range of operating scenarios and not dependent on how the lithium is introduced to the PFC or plasma edge. Scans of toroidal field, plasma current and magnetic field configuration have been performed. A slight increase in the average impurity concentration, probably caused by an improvement in confinement, is observed when either the magnetic field or the plasma current are increased. Projections to future devices with higher field and current than NSTX indicate that techniques must be developed to limit such an accumulation of impurity, especially for long-pulse operations.

The lithium content in the confined plasma for different conditions at the plasma–wall interface has also been investigated by varying the amount of lithium evaporated into the vessel prior or during a discharge and by varying the temperature of the LLD well above the nominal melting temperature for pure lithium. In spite of the very different conditions induced at the plasma–PFC interface, no substantial trend is observed in the core lithium concentration with any of those parameters.

The only case for which a large increase of the core lithium concentration is observed is during anomalous events. For instance, a transient accumulation of lithium is observed when the plasma interacts with a macroscopic, localized conglomerate of lithium located in the divertor region. It should be emphasized that, although in this case n_{Li} is larger than in typical NSTX plasmas, its contribution to plasma contamination remains nevertheless modest. For instance, $n_{\mathrm{Li}}/n_{\mathrm{e}} \sim 0.2\%$ would cause an increase in Z_{eff} of only $\Delta Z_{\mathrm{eff}} \approx 0.012$.

In conclusion, lithium concentration in the core plasma of NSTX remains extremely low, even after a large amount of lithium, of the order of hundreds of milligrams, is evaporated on the PFCs. Upper limits inferred from the experiments are well below 0.1% of the electron density in the measurement region, ranging from the plasma mid-radius ($R \approx 120$ cm) out to the edge ($R = 140$–145 cm). Consistently with previous measurements [7], carbon remains the dominant impurity for NSTX plasmas. The physical mechanisms behind the different behaviour of carbon and lithium are still under investigation. A plausible hypothesis is that lithium influx from the PFCs to the main plasma is inhibited by its low ionization potential ($\approx$5.4 eV) compared with carbon ($\approx$11.3 eV), which favours redeposition resulting in increased retention of lithium in the divertor region, hence a reduced core contamination [27]. Other mechanisms, such as the outward diffusion of lithium caused by collisions on the higher-Z, higher density carbon ions, may also prevent lithium accumulation in the core. The results of this ongoing research will be presented in future works.

Acknowledgments

The authors would like to thank Drs S.A. Sabbagh and J.E. Menard for the equilibrium reconstructions used in this paper and Dr A. McLean for the LLD temperature data. The valuable contribution of the NSTX Neutral Beam group and the LITER/Li-dropper operators is gratefully acknowledged. Work supported by DOE grant no DE-AC02-09CH11466.

References

[1] Loarte A. *et al* 2007 ITER physics basis, chapter 4: Power and particle control *Nucl. Fusion* **47** S203

[2] Mansfield D.K. *et al* 2001 Observations concerning the injection of a lithium aerosol into the edge of TFTR discharges *Nucl. Fusion* **41** 1823

[3] Mirnov S.V. *et al* 2003 Li-CPS limiter in tokamak T-11M *Fusion Eng. Des.* **65** 455

[4] Mazzitelli G. *et al* 2011 FTU results with a liquid lithium limiter *Nucl. Fusion* **51** 073006

[5] Sánchez J. *et al* 2009 Impact of lithium-coated walls on plasma performance in the TJ-II stellarator *J. Nucl. Mater.* **390–391** 852

[6] Ono M. *et al* 2000 Exploration of spherical torus physics in the NSTX device *Nucl. Fusion* **40** 557

[7] Bell M.G. *et al* 2009 Plasma response to lithium-coated plasma-facing components in the national spherical torus experiment *Plasma Phys. Control. Fusion* **51** 124054

[8] Ono M. *et al* 2010 Implications of NSTX lithium results for magnetic fusion research *Fusion Eng. Des.* **85** 882

[9] Maingi R. *et al* 2011 Continuous improvement of H-mode discharge performance with progressively increasing lithium coatings in the National Spherical Torus Experiment *Phys. Rev. Lett.* **107** 145004

[10] Ono M. *et al* 2011 Recent progress of NSTX lithium program and opportunities for magnetic fusion research *Fusion Eng. Des.* http://dx.doi.org/10.1016/j.fusengdes.2011.10.011

[11] Kugel H.W. *et al* 2011 NSTX plasma operation with a Liquid Lithium Divertor, *Fusion Eng. Des.* http://dx.doi.org/10.1016/j.fusengdes.2011.07.010

[12] Kugel H.W. *et al* 2008 The effect of lithium surface coatings on plasma performance in the National Spherical Torus Experiment *Phys. Plasmas* **15** 056118

[13] Kugel H.W. *et al* 2010 Lithium coatings on NSTX plasma facing components and its effects on boundary control, core plasma performance, and operation *Fusion Eng. Des.* **85** 865

[14] Mansfield D.K. *et al* 2010 A simple apparatus for the injection of lithium aerosol into the scrape-off layer of fusion research devices *Fusion Eng. Des.* **85** 890

[15] Nygren R.E. *et al* 2011 Preparation of the liquid lithium divertor plates for NSTX *J. Nucl. Mater.* **417** 592

[16] Mirnov S.V. *et al* 2011 Li experiments on T-11M and T-10 in support of a steady-state tokamak concept with Li closed loop circulation *Nucl. Fusion* **51** 073044

[17] Zakharov L.E. *et al* 2007 Low recycling regime in ITER and the LiWall concept for its divertor *J. Nucl. Mater.* **363–365** 453

[18] Menard J.E. *et al* 2010 Physics design of the NSTX upgrade *Proc. 37th EPS Conf. on Plasma Physics* vol 34F (Belfast, Ireland, 2010) P–2.106 http://ocs.ciemat.es/EPS2010PAP/pdf/P2.106.pdf

[19] Bell R.E. *et al* 2010 Comparison of poloidal velocity measurements to neoclassical theory on NSTX *Phys. Plasmas* **17** 082507

[20] Johnson R.C. 1927 The structure and origin of the Swan band spectrum of carbon *Phil. Trans. R. Soc. Lond.* A **226** 157

[21] Bell R.E. *et al* 2000 New understanding of poloidal rotation measurements in a tokamak plasma 12th Topical Conf. on Atomic Processes in Plasmas ed R.C. Mancini *et al AIP Conf. Proc.* **547** 39 http://proceedings.aip.org/resource/2/apcpcs/547/1/39_1

[22] Maingi R. *et al* 2009 Edge-localized-mode suppression through density-profile modification with lithium-wall coatings in the National Spherical Torus Experiment *Phys. Rev. Lett.* **103** 075001

[23] Kaye S.M. *et al* 2007 Confinement and local transport in the National Spherical Torus Experiment (NSTX) *Nucl. Fusion* **47** 499

[24] Soukhanovskii V.A. *et al* 2009 Divertor heat flux mitigation in the National Spherical Torus Experiment *Phys. Plasmas* **16** 022501

[25] Soukhanovskii V.A. *et al* 2011 Taming the plasma–material interface with the snowflake divertor in NSTX *Nucl. Fusion* **51** 012001

[26] Canik J.M. *et al* 2010 Progress in the development of ELM pace-making with non-axisymmetric magnetic perturbations in NSTX *Nucl. Fusion* **50** 064016.

[27] Allain J.P. *et al* 2011 Lithium surface-response modelling for the NSTX liquid lithium divertor *Nucl. Fusion* **51** 023002